Electronic Supplementary Material (ESI) for Chemical Communications.
This journal is © The Royal Society of Chemistry 2023

Modulating the doping state of transition metal ions in ZnS for enhanced photocatalytic activity

Linping Bao,[a] Xiaohui Ren,[b] Chengyin Liu,[c] Xin Liu,*[,a] Chunhui Dai,[d] Yong Yang,[e] Mohamed Bououdina,[f] Sajjad Ali,*[,g] Chao Zeng*[,a]

[a] Institute of Advanced Materials, College of Chemistry and Chemical Engineering, Key Lab of Fluorine and Silicon for Energy Materials and Chemistry of Ministry of Education, Jiangxi Normal University, Nanchang 330022, PR China

[b] The State Key Laboratory of Refractories and Metallurgy, School of Materials and Metallurgy, Wuhan University of Science and Technology, Wuhan 430081, PR China

[c] School of Environmental and Material Engineering, Yantai University, Yantai 264005, PR China

[d] Jiangxi Key Laboratory for Mass Spectrometry and Instrumentation, East China University of Technology, Nanchang 330013, PR China

[e] Jiangxi Key Laboratory of Nanomaterials and Sensors, Jiangxi Key Laboratory of Photoelectronics and Telecommunication, School of Physics, Communication and Electronics, Jiangxi Normal University, Nanchang, Jiangxi Province, 330022, PR China

[f] Department of Mathematics and Sciences, College of Humanities and Sciences, Prince Sultan University, Riyadh 11586, Saudi Arabia

[g] Energy, Water, and Environment Lab, College of Humanities and Sciences, Prince Sultan University, Riyadh 11586, Saudi Arabia

*E-mail: liuxin@jxnu.edu.cn, sajjad@alum.imr.ac.cn, czeng@jxnu.edu.cn

Contents

1. Experimental Section

1.1 Preparation of the photocatalyst.

Synthesis of ZnS. ZnS was prepared by a facile water bath method. In brief, $ZnCl_2$ and thioacetamide (TAA) with molar ratio of 1:1 were dispersed into 30 mL of distilled water. After continuous stirring for 30 min at room temperature, the resulting mixture was subjected to water bath at 80 °C for 5 h under magnetic stirring. After cooling naturally to room temperature, the obtained products were centrifuged and washed using distilled water for three times. Then, after freeze-drying for two days, the final products were grounded with a mortar.

Synthesis of H-MZnS-X (M = Cu, Co, Ag and Cr). The details for preparing transition metal ions homogeneous doped in ZnS (H-MZnS-X) were as follows. Taking Cu homogeneous doped ZnS as an example, a certain amount of $ZnCl_2$, TAA and $CuCl_2\cdot 2H_2O$ were dispersed into 30 mL of distilled water firstly. The mixture was stirred magnetically at room temperature for 30 min, then transferred to a Teflon lined autoclave (50 mL) and reacted for 12 h at 120 °C in an oven. After cooling to room temperature, the resultant product was collected by centrifugation and washed with distilled water for three times. After freeze-drying and grinding, the H-CuZnS-X was obtained (X = 1, 2, 3, 4, 5, and 6, X denotes different molar ratios of added $CuCl_2/ZnCl_2$, and the actual Cu^{2+}/Zn^{2+} molar ratios were obtained by ICP test, as shown in Figure S1). The H-CoZnS (the molar ratio of added $Co(NO_3)_2$ to $ZnCl_2$ is 6%), H-AgZnS (the molar ratio of added $AgNO_3$ to $ZnCl_2$ is 2%) and H-CrZnS (the molar ratio of added $Cr(NO_3)_3$ to $ZnCl_2$ is 6%) were fabricated following the same procedure while replacing $CuCl_2\cdot 2H_2O$ with $Co(NO_3)_2$, $AgNO_3$ and $Cr(NO_3)_3$, respectively, and the preparation temperature for H-CrZnS was increased up to 180 °C.

Synthesis of S-MZnS-X (M = Cu, Co, Ag and Cr). The surface doped ZnS (S-

MZnS-X) were synthesized as follows. Take Cu surface doped ZnS as an example, a certain amount of the as-prepared ZnS was dispersed in 30 mL of distilled water, and then was subjected to ultrasonication for 5 min. A certain amount of $CuCl_2·2H_2O$ was added to the above suspension with magnetic stirring for 30 min. Next, the mixture was transferred to a Teflon lined autoclave (50 mL) and reacted for 12 h at 120 ℃ in an oven. After cooling to room temperature, the resultant product was collected by centrifugation and washed with distilled water for three times. After freeze-drying and grinding, the S-CuZnS-X (X = 1, 2, 3, 4, and 5, X denotes different molar ratios of added $CuCl_2$ to $ZnCl_2$, the actual Cu^{2+}/Zn^{2+} molar ratios were obtained by ICP test, as shown in Figure S1) was obtained. The H-CoZnS (the molar ratio of added $Co(NO_3)_2$ to $ZnCl_2$ is 8%), H-AgZnS (the molar ratio of added $AgNO_3$ to $ZnCl_2$ is 5%) and H-CrZnS (the molar ratio of added $Cr(NO_3)_3$ to $ZnCl_2$ is 2%) were fabricated following the same procedure while replacing $CuCl_2·2H_2O$ with $Co(NO_3)_2$, $AgNO_3$ and $Cr(NO_3)_3$ respectively, and the preparation temperature for S-CrZnS was increased up to 180 ℃.

1.2 Characterization.

X-ray diffraction (XRD) measurement was performed on a Bruker D8 focus with Cu Kα radiation at a scanning speed of 4°/min. Raman spectra were recorded on a Renishaw instrument equipped with a 532 nm laser. X-ray photoelectron spectroscopy (XPS) analysis was carried out on an ESCALAB 250xi (Thermo Fisher, England) electron spectrometer. Scanning electron microscopy (SEM) images were obtained by a Hitachi SU8020 operating at 20 kV. Transmission electron microscopy (TEM) observations were conducted on a JEM-2100. UV-vis diffuse reflectance spectra (DRS) were recorded on a UV-vis spectrometer (Hitachi U-3310) using $BaSO_4$ as a reference. The specific surface areas (S_{BET}) and pore diameter distribution were determined by nitrogen adsorption and desorption isotherm method using a Micromeritics TriStar II

3020 apparatus. Static water contact-angle was measured on an OCA50 instrument. Steady-state and time-resolved photoluminescence spectra were recorded on a fluorescence spectrophotometer (Edinburgh FLS980). The electron paramagnetic resonance (EPR) spectra were measured on a Endor spectrometer (Bruker JES FA200) at 77 K. Element content analysis was performed using an inductively coupled plasma-mass spectrometry (ICP-MS) (Agilent ICPOES730).

1.3 Photocatalytic Tests.

The photocatalytic H_2 evolution activity of the obtained powdered samples was examined in an on-line closed cycle system with a catalyst dosage of 50 mg. In addition, 50 mL of a 0.35 M Na_2S-0.25 M Na_2SO_3 aqueous solution acted as a sacrificial agent, and Pt (1 wt %) worked as a cocatalyst, which was in situ photo-deposited on the surface of the catalyst by dissolving H_2PtCl_6 in the solution containing catalyst and sacrificial agent. After ultrasonication for 5 min, the mixture was transferred to a photoreactor (Pyrex glass), which is connected to a closed-cycle gas circulation system and a vacuum line (MC-SPH2O-AG, Merry Change, Beijing). Before photoreaction, the entire glass tube was vacuumed for 30 min to remove any residual air. The reaction was maintained at 6 °C by a circulating condensation system. The generated hydrogen was quantified by an on-line gas chromatograph equipped with a thermal conductivity detector (GC9709 II, Fuli, Zhejiang, Ar carrier), which is matched with the photocatalytic hydrogen production system.

The photocatalytic CO_2 reduction was performed in a quartz reaction cell. First, 20 mg of catalyst was dispersed in 3 mL ultra-pure water, and then the obtained suspension was evenly dropped on a quartz dish and then placed in the oven at 60 °C. After drying, the quartz dish covered with catalyst was put into the reactor, sealed, vacuum treated, and then filled with high purity CO_2 (99.999%) to achieve atmospheric pressure, and 2 mL of ultrapure water was injected into the reactor. The photocatalytic CO_2 reduction reaction was carried out under the irradiation of 300 W xenon lamp, and the resultant product was analyzed by a gas chromatograph (GC 9790II, FID detector).

1.4 Photoelectrochemical Characterization.

10 mg catalyst was ultrasonically dispersed in 800 μL ethanol by ultrasound, and then the mixture was slowly dripped onto ITO glass sheets. After natural withering, the working electrode was obtained. Photoelectrochemical experiment was conducted in a standard three-electrode cell. Platinum and Ag/AgCl were used as counter electrode and reference electrode, respectively, and 0.1M Na_2SO_4 was used as the electrolyte. EIS Nynquist plots, photocurrent response, and linear sweep voltammetry (LSV) measurements were conducted on a CS315H workstation. The Mott-Schottky curves were recorded on a CHI760E workstation.

1.5 Computational Modelling.

Density functional theory (DFT) calculations were performed using Vienna ab initio simulation package (VASP).[1,2] The Perdew-Burke-Ernzerhof (PBE)[3] functional with generalized gradient approximation (GGA) are used for the exchange-correlation potentials. For structure optimization, 3×3×1 k-points mesh and 450 eV energy cutoff have been used. The DFT-D3 type of van der Waals correction are considered in the DFT calculations.[4]

The ZnS periodic cell comprised 54 atoms (27 zinc and 27 sulfur atoms), and a vacuum space was kept at ~14.4 Å. The ZnS supercell is rhombohedral $11.53\times 11.53\times 23.04$ Å^3 for x, y, and z directions, with $\alpha=\beta = 90°$ and $\gamma= 120°$. Moreover, ZnS is periodic along the x and y directions. The energy convergence criteria were set to 1×10^{-5} eV to get accurate forces, and a force tolerance of -0.02 eV/Å was used in structural optimization.

The hydrogen evolution reaction (HER) proceeds via one-electron transfer mechanism and includes one proton-electron coupled elementary steps:

$$H^{+} + e^{-} + * \rightarrow H* \qquad (3)$$

$$H* \rightarrow \frac{1(H2)}{2} + * \qquad (4)$$

where $*$ indicates ZnS active site, and $H*$ is the H adsorption. The zero-point energy, enthalpy, and entropy corrections were added to $H*$ to convert electronic energy of $H*$ to free energy.

The Gibbs free energy (G) at U=0 V is modified by Equation (5).

$$\mathrm{G} = E_{DFT} + E_{ZPE} - TS + \int \mathrm{C_p d}T \qquad (5)$$

where E_{DFT}, E_{ZPE}, TS, and $\int \mathrm{C_p d}T$ represent electronic energy, zero-point energy room temperature entropy and heat capacity (i.e., T=298.15 K). The Gibbs free energy was calculated using the computational hydrogen electrode (CHE) model. In CHE model, the reaction step proton-electron coupled and the G of electron-proton pairs (e^{-} + H^{+}) was calculated as a function of applied potential (U) relative to a reversible hydrogen electrode (RHE),[5] i.e., $\mu(H^{+}) + \mu(e^{-}) = \frac{1}{2}\mu(H_2) - eU$. The G of the adsorbed hydrogen ΔG(H*) is a key descriptor for the HER catalytic activity, and ΔG(H*) at a given potential U_{RHE} can be written as:

$$\Delta G(\mathrm{H}*) = G(\mathrm{H}*) - G(*) - \frac{1G(H2)}{2} - eU_{RHE} \qquad (6)$$

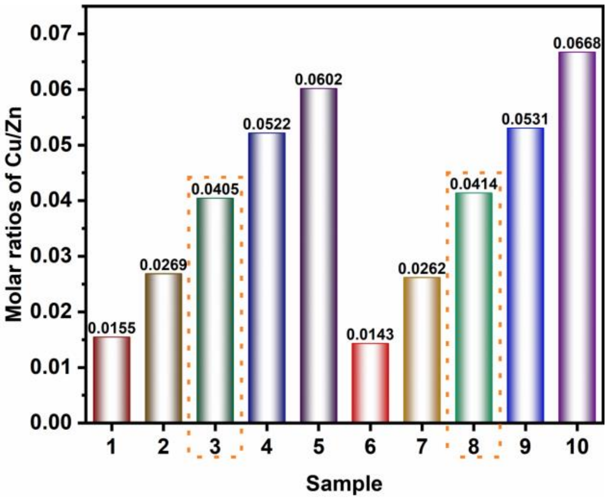

Figure S1. Molar ratios of Cu/Zn for Cu-doped ZnS calculated by ICP-MS (samples 1-10 represent H-CuZnS-1, H-CuZnS-2, H-CuZnS-3, H-CuZnS-4, H-CuZnS-5, S-CuZnS-1, S-CuZnS-2, S-CuZnS-3, S-CuZnS-4, and S-CuZnS-5, respectively). The H-CuZnS-3 and S-CuZnS-3 (marked with light orange dotted rectangle) with same actual Cu/Zn molar ratios of ~ 0.041 are marked as H-CuZnS and S-CuZnS.

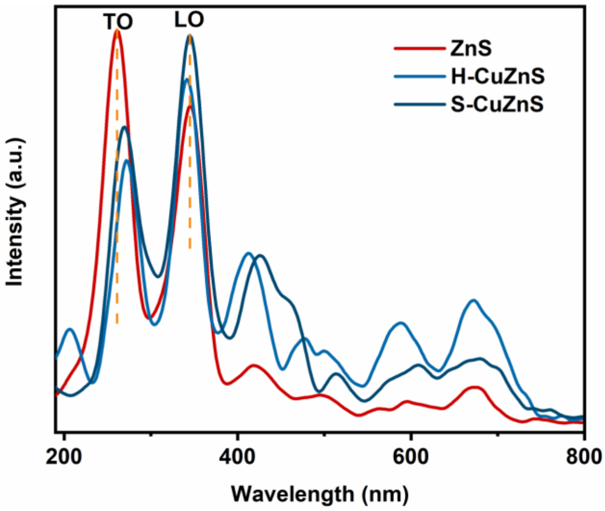

Figure S2. Raman spectra for ZnS, H-CuZnS and S-CuZnS.

Besides, Raman spectroscopy has been utilized to investigate the structure of catalysts. As shown in Figure S2, the main peaks of 261.4 and 345.2 cm-1 can be assigned to the transverse optical (TO) and longitudinal optical (LO) phonon modes of pure ZnS, respectively. After Cu doping, the Raman peaks of TO mode is obviously attenuated because of the distortion of structural symmetry,[6] and the ascended peaks for LO mode at 400-800 cm-1 can be attributed to the strengthened polarity and crystallinity.[7] Relative to the pristine ZnS, H-CuZnS shows a greater variation of Raman spectrum than S-CuZnS, suggesting the more structural symmetry damage of Cu homogeneous doping to surface doping.

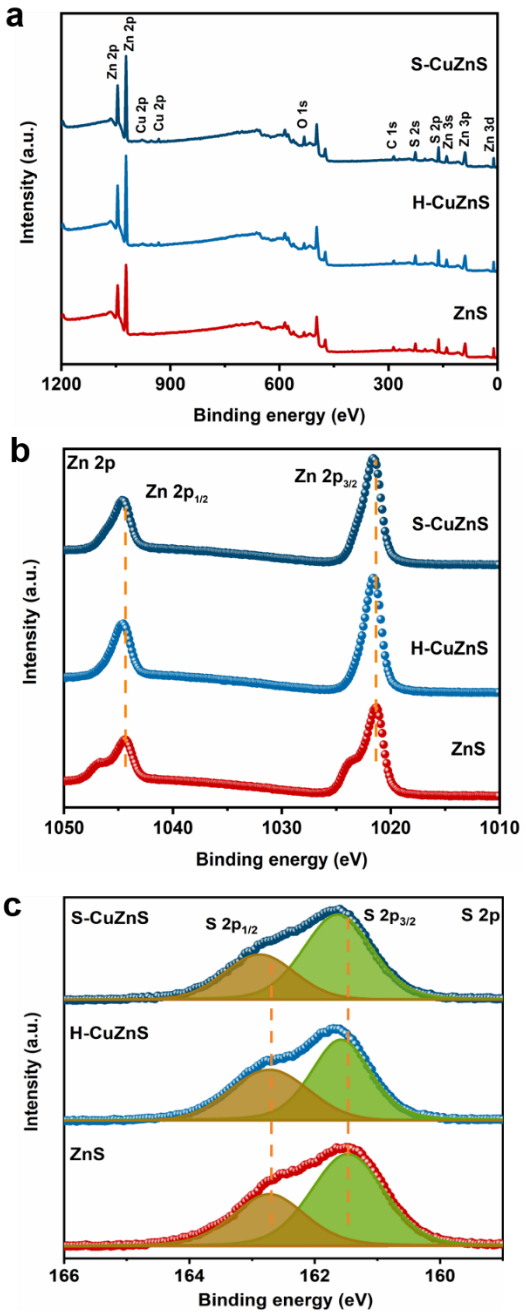

Figure S3. (a) Typical XPS survey spectra, high-resolution XPS spectra of (b) Zn 2p, and (c) S 2p for ZnS, H-CuZnS and S-CuZnS.

Table S1. Atomic percentages of the Zn, S and Cu elements on the surface of ZnS, H-CuZnS and S-CuZnS calculated by their corresponding XPS spectra.

Elements	ZnS	H-CuZnS	S-CuZnS
Zn (Atomic %)	45.36	44.02	43.26
S (Atomic %)	33.27	34.55	33.3
Cu (Atomic %)	0	1.8	1.81

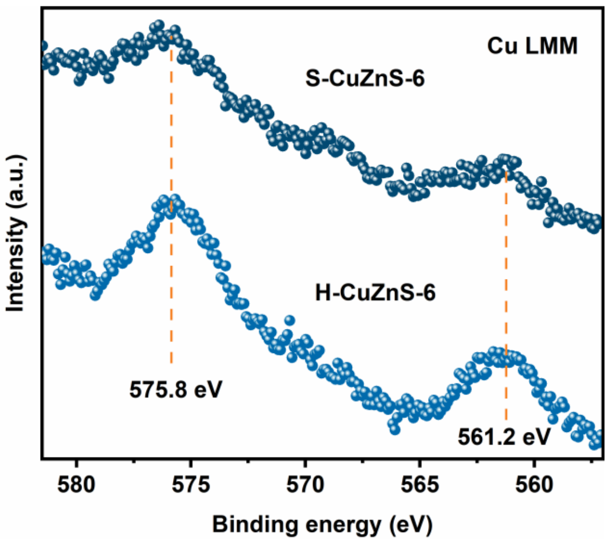

Figure S4. High-resolution Cu LMM spectra for H-CuZnS-6 and S-CuZnS-6.

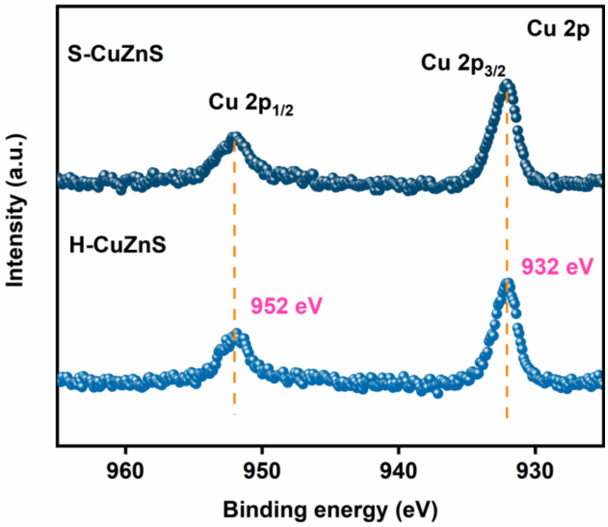

Figure S5. High-resolution Cu 2p spectra for H-CuZnS and S-CuZnS.

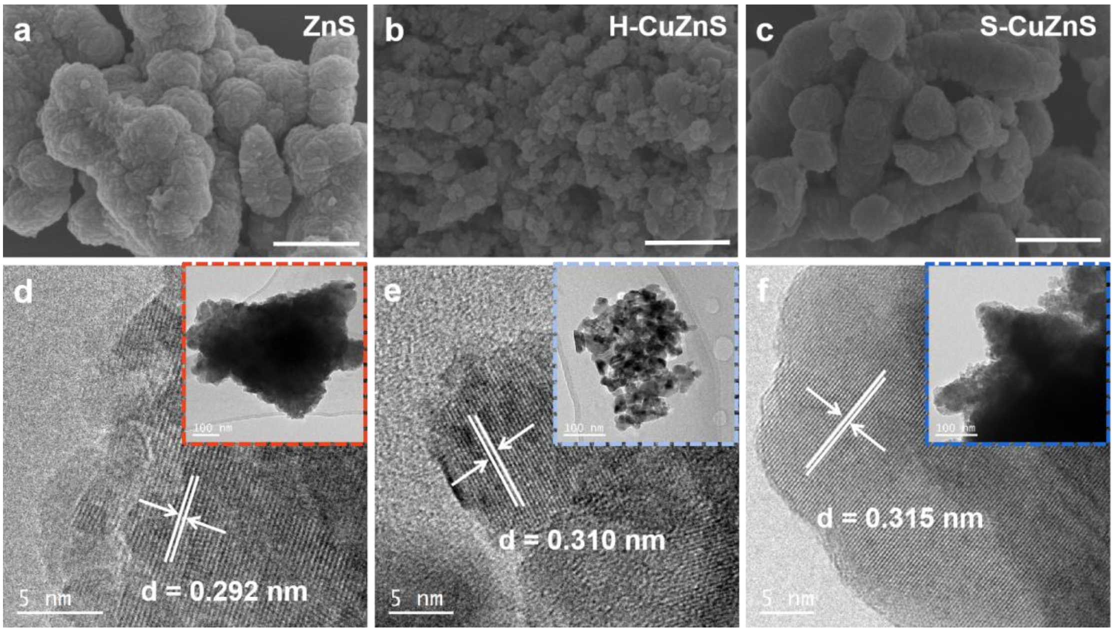

Figure S6. SEM images of (a) ZnS, (b) H-CuZnS and (c) S-CuZnS, and the scale bar of the inset is 500 nm. HRTEM images of (d) ZnS, (e) H-CuZnS and (f) S-CuZnS, and the insets are the TEM image.

The morphology and microstructure of the as-obtained catalysts were analyzed by SEM and TEM. The SEM image in Figure S6a depicts that ZnS are composed of many nanosheets, and the introduction of Cu or Co dopants have no obvious effect on the morphology of ZnS (Figure S6b-c, Figure S7). The TEM and HRTEM images of ZnS, H-CuZnS, and S-CuZnS as shown in Figure S6d-f, further prove that ZnS and Cu-doped ZnS are aggregates of nanosheets. The lattice fringes of ZnS, H-CuZnS, and S-CuZnS are determined to be 0.29 nm, 0.31 nm, and 0.31nm, respectively, coinciding with the (012) plane of hexagonal ZnS.

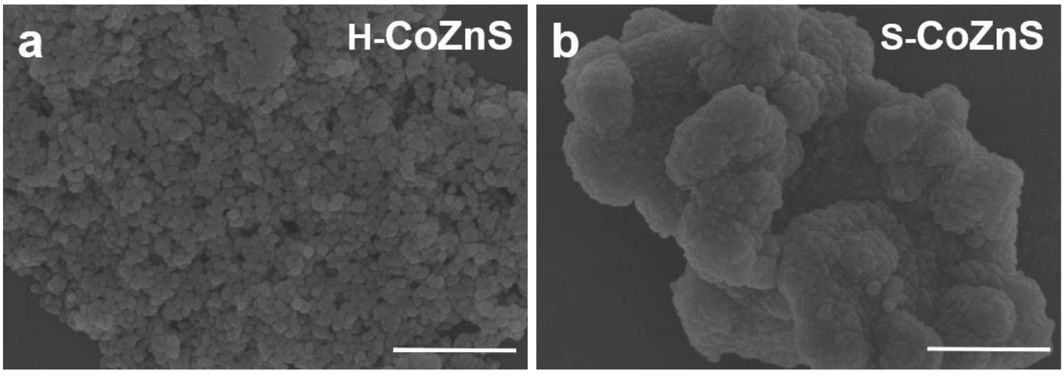

Figure S7. SEM images of (a) H-CoZnS, and (b) S-CoZnS, and the scale bar of the inset is 500 nm.

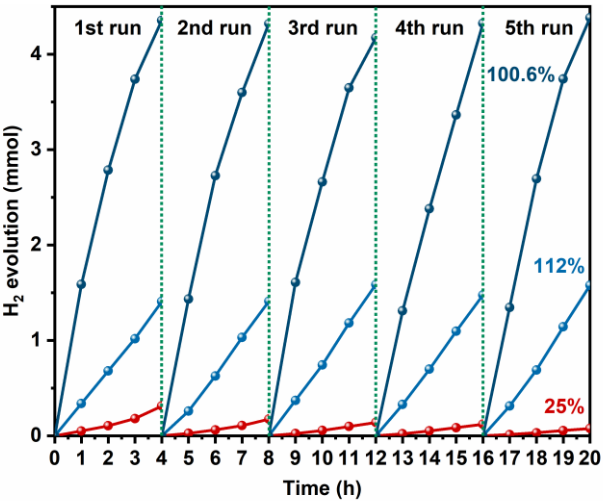

Figure S8. Cycling runs for photocatalytic H_2 evolution for ZnS (red), H-CuZnS (light blue) and S-CuZnS (dark blue).

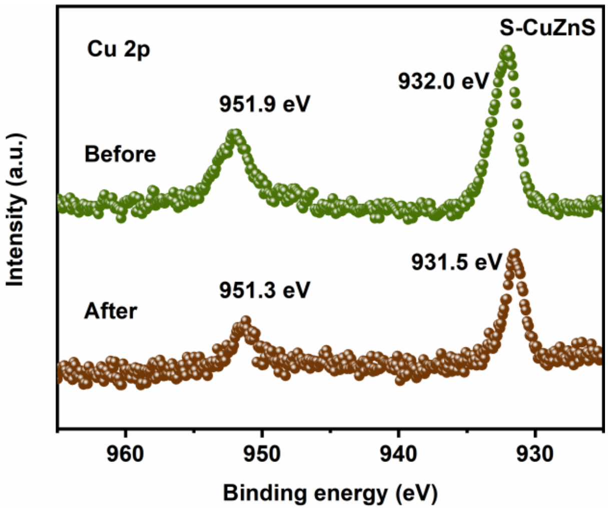

Figure S9. High-resolution XPS spectra of Cu 2p for S-CuZnS before and after circular reaction.

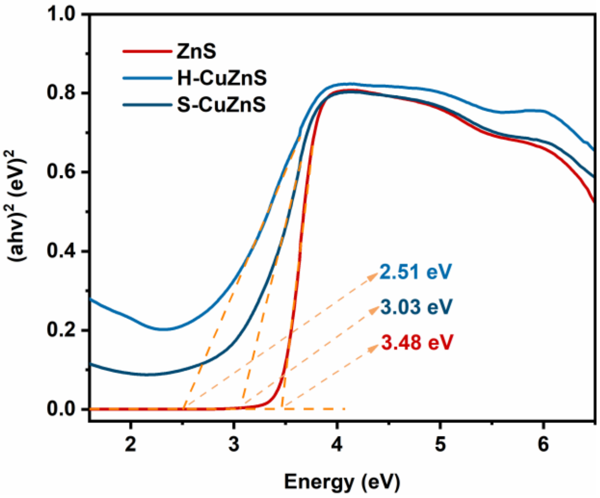

Figure S10. Band gaps for ZnS, H-CuZnS, and S-CuZnS.

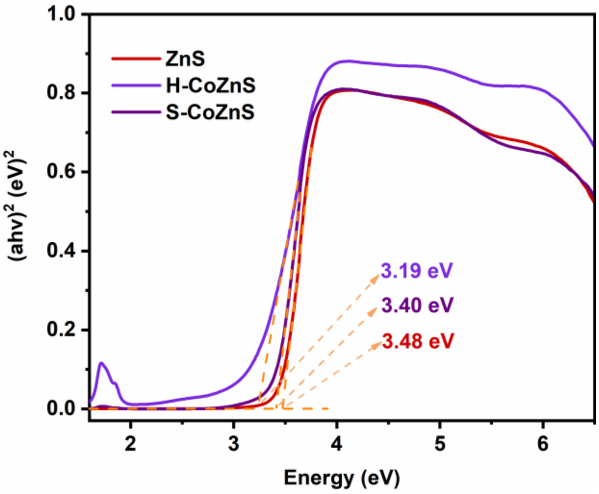

Figure S11. Band gaps for ZnS, H-CoZnS, and S-CoZnS.

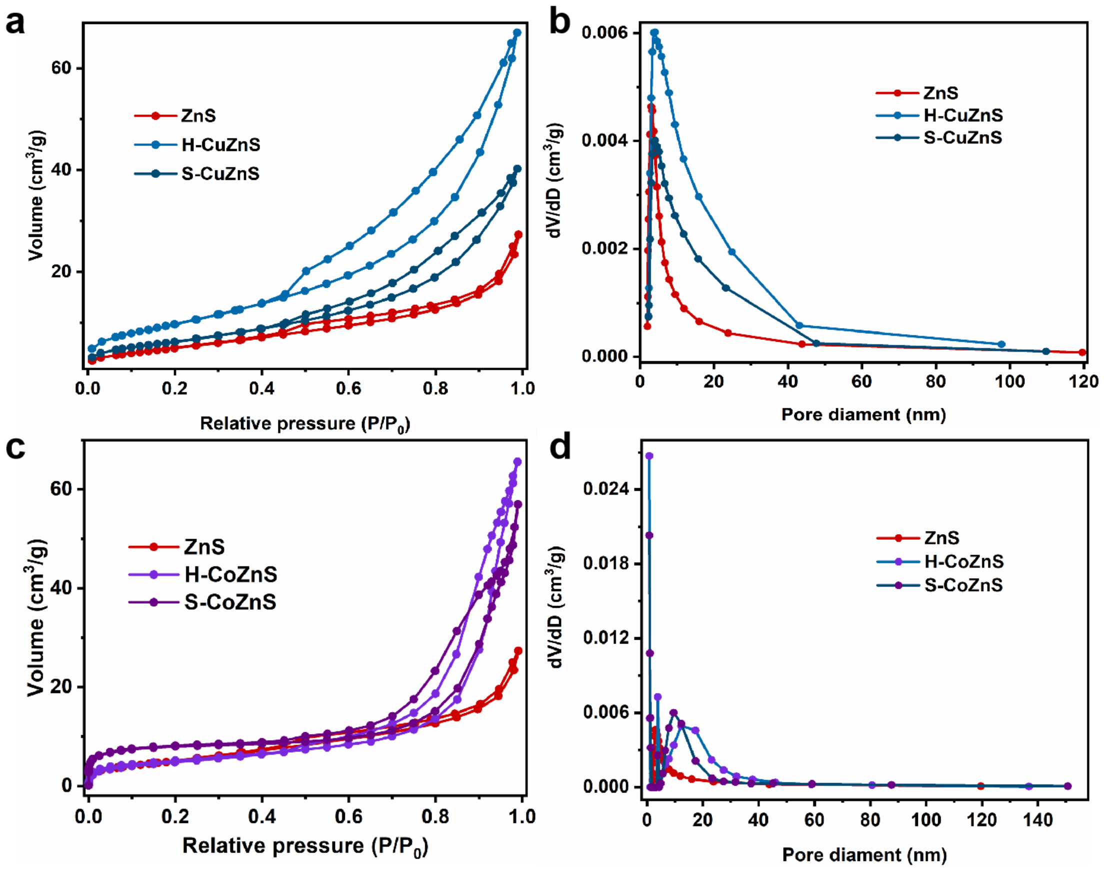

Figure S12. (a, c) Nitrogen adsorption/desorption isotherms and (b, d) pore diameter distribution of ZnS, H-MZnS and S-MZnS.

The specific surface area and porosity of the as-obtained catalysts are investigated based on Brunauer-Emmett-Teller and Barrett-Joyner-Halenda (BET/BJH) methods. The as-obtained catalysts exhibit a typical II isotherm (Figure S12a),[8] and the S_{BET} of ZnS, H-CuZnS, and S-CuZnS are measured to be 19.1, 37.0 and 23.6 m^2/g, respectively. The average pore diameters of ZnS, H-CuZnS and S-CuZnS are 8.4, 10.3 and 9.9 nm, respectively (Figure S12b). As for H-CoZnS and S-CoZnS samples, S_{BET} is slightly smaller than ZnS (Figure S12c), but their average pore diameters are significantly larger than ZnS (Figure S12d). In general, the larger specific surface area can provide more active sites for photoreaction,[9] which is beneficial for photocatalysis. However, the S-MZnS with smaller S_{BET} compared to H-MZnS, possesses higher activity, validating the positive effect of surface doping.

Table S2. The S_{BET} and average pore diameter of ZnS, H-MZnS and S-MZnS photocatalysts determined by nitrogen adsorption and desorption method.

Photocatalyst	S_{BET} (m^2/g)	Average pore diameter (nm)
ZnS	19.1	8.4
H-CuZnS	37.0	10.3
S-CuZnS	23.6	9.9
H-CoZnS	18.3	22.2
S-CoZnS	11.9	29.6

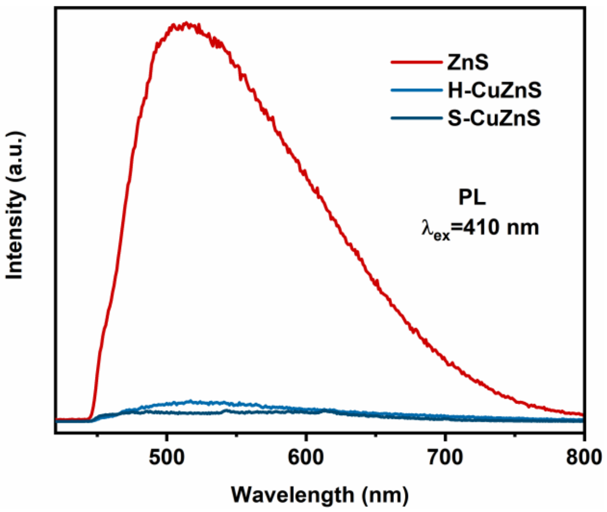

Figure S13. PL spectra for ZnS, H-CuZnS and S-CuZnS.

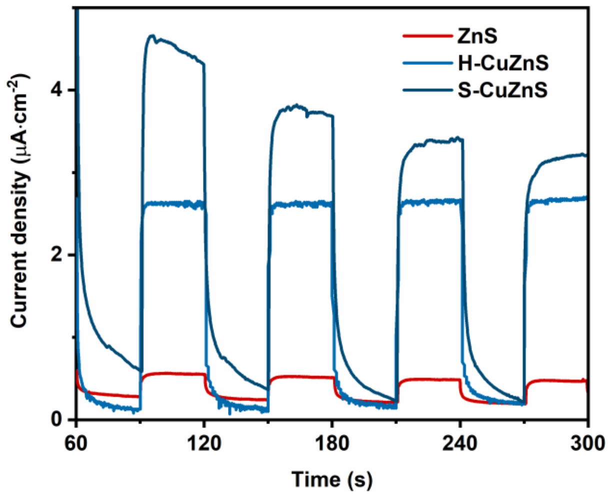

Figure S14. Transient photocurrent responses for ZnS, H-CuZnS and S-CuZnS.

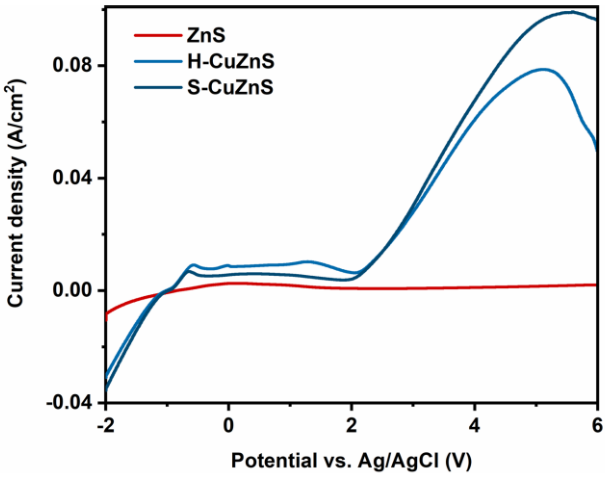

Figure S15. LSV for ZnS, H-CuZnS, and S-CuZnS.

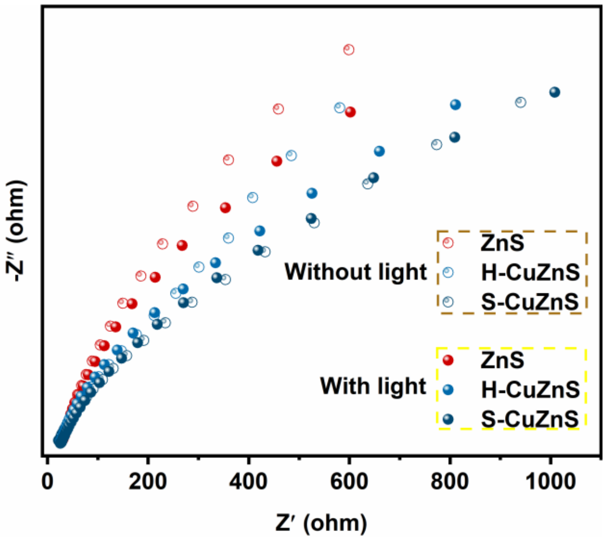

Figure S16. EIS Nyquist plots for ZnS, H-CuZnS and S-CuZnS.

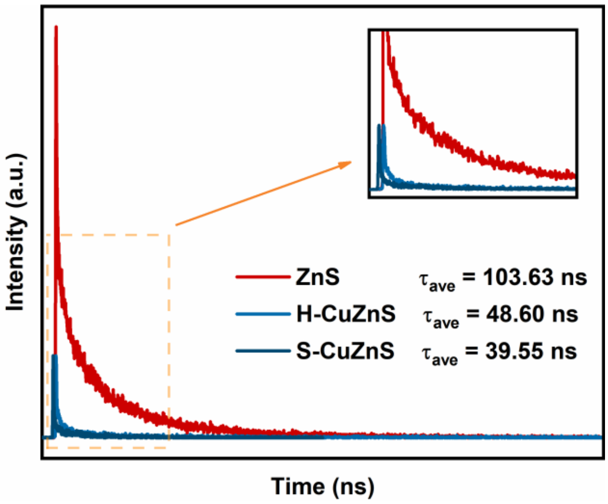

Figure S17. Photoluminescence decay curves for ZnS, H-CuZnS and S-CuZnS.

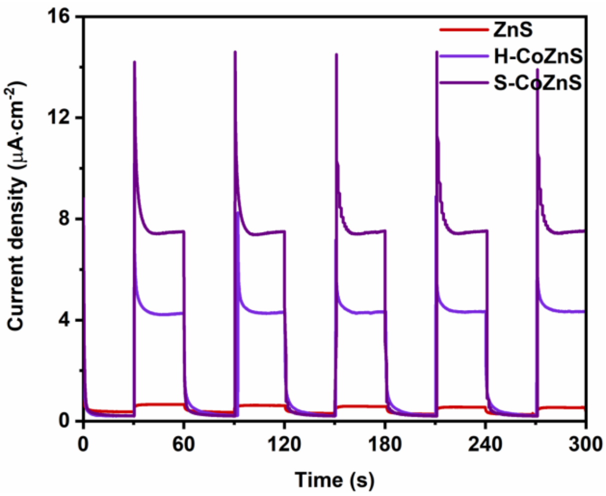

Figure S18. Transient photocurrent responses for ZnS, H-CoZnS and S-CoZnS.

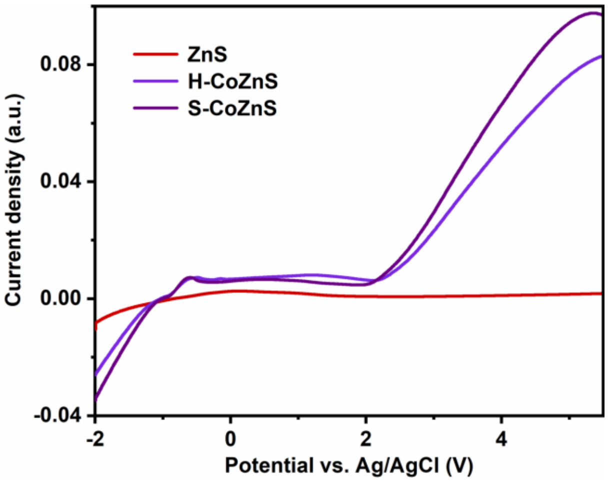

Figure S19. LSV for ZnS, H-CoZnS and S-CoZnS.

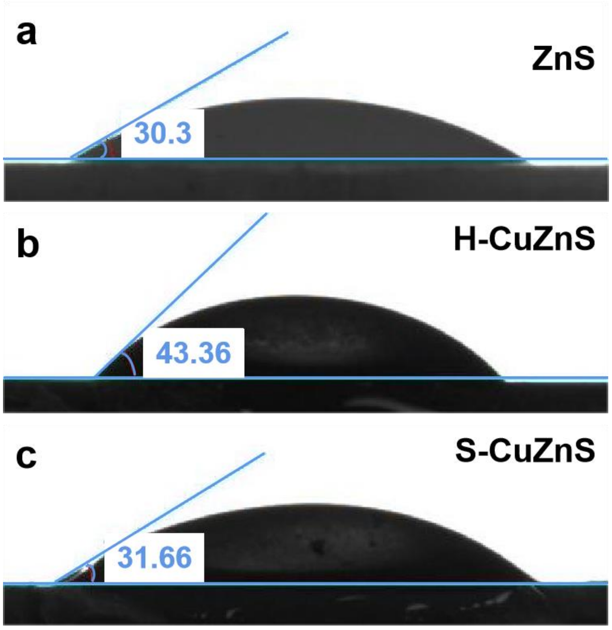

Figure S20. Static water contact-angle measurement of ZnS, H-CuZnS and S-CuZnS.

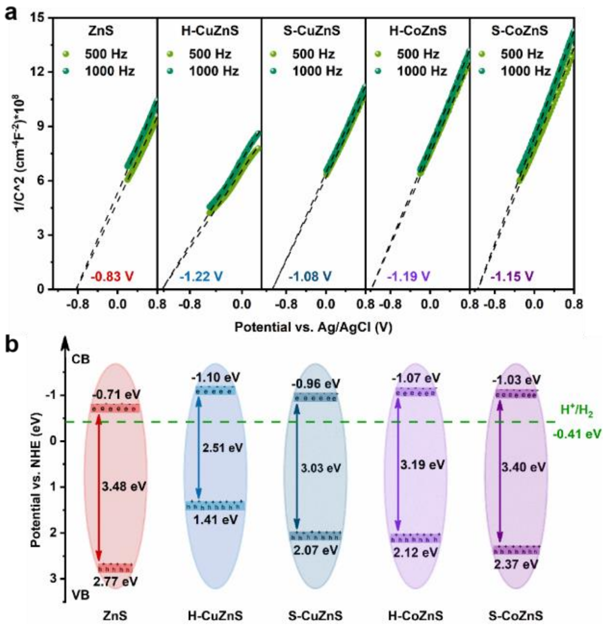

Figure S21. (a) Mott-Schottky curves and (b) band structures for ZnS, H-MZnS, and S-MZnS (M = Cu^{2+}, Co^{2+}).

The band structure of ZnS and ions doped ZnS are investigated based on Mott-Schottky curves. The positive slope of the Mott-Schottky curves (Figure 21a) indicates the n-type semiconductors of the as-obtained catalysts.[10] The flat band potential values (E_{fb}) of ZnS, H-CuZnS, S-CuZnS, H-CoZnS and S-CoZnS are calculated to be -0.83 V, -1.22 V, -1.08 V, -1.19 V, and -1.15 V versus Ag/AgCl, respectively. According to the following transformation equation between normal hydrogen electrode (NHE) and Ag/AgCl electrode: $E_{vs.NHE} = E_{vs.Ag/AgCl} + 0.22$ V,[11] the E_{fb} of ZnS, H-CuZnS, S-CuZnS, H-CoZnS and S-CoZnS are -0.61 V, -1.00 V, -0.86 V, -0.97 V, and -0.93 V versus NHE, respectively. The E_{fb} of n-type semiconductors is generally considered to be 0.1 V more positive than the CB potential (E_{CB}).[12] As a consequence, the E_{CB} of ZnS, H-CuZnS, S-CuZnS, H-CoZnS and S-CoZnS are determined to be -0.71 V, -1.1 V, -0.96 V, -1.07 V, and -1.03 V versus NHE, respectively. Based on the Eg calculated from DRS in Figure S10-11, the valence band potential (E_{VB}) of ZnS, H-CuZnS, S-CuZnS, H-CoZnS and S-CoZnS are estimated to be 2.77 V, 1.41 V, 2.07 V, 2.12 V, and 2.37 V, respectively. Therefore, the schematic diagram of energy band structure for ZnS and ions doped ZnS are depicted in Figure S21b. Compared to the pristine ZnS, H-MZnS exhibit greater difference of band structures to S-MZnS, which also demonstratse that homogeneous doping has greater damage to the electronic structure.

Table S3. Band gap comparison between experiment and DFT.

System	**Experiment**	**DFT**
ZnS	3.48	3.46
H-CuZnS	2.51	2.35
S-CuZnS	3.03	3.01
H-CoZnS	3.19	2.53
S-CoZnS	3.40	3.30

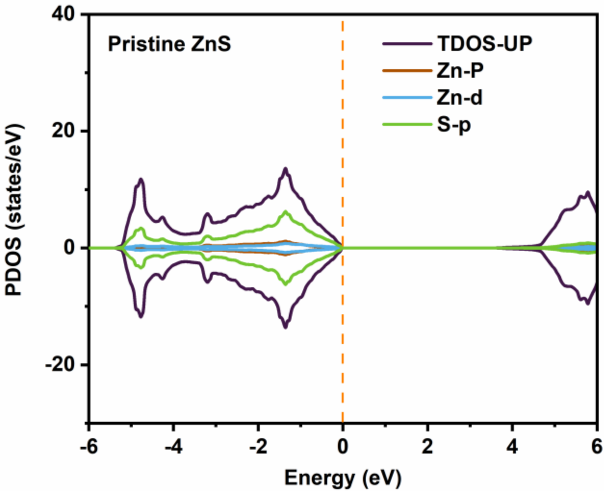

Figure S22. Density of states for pristine ZnS.

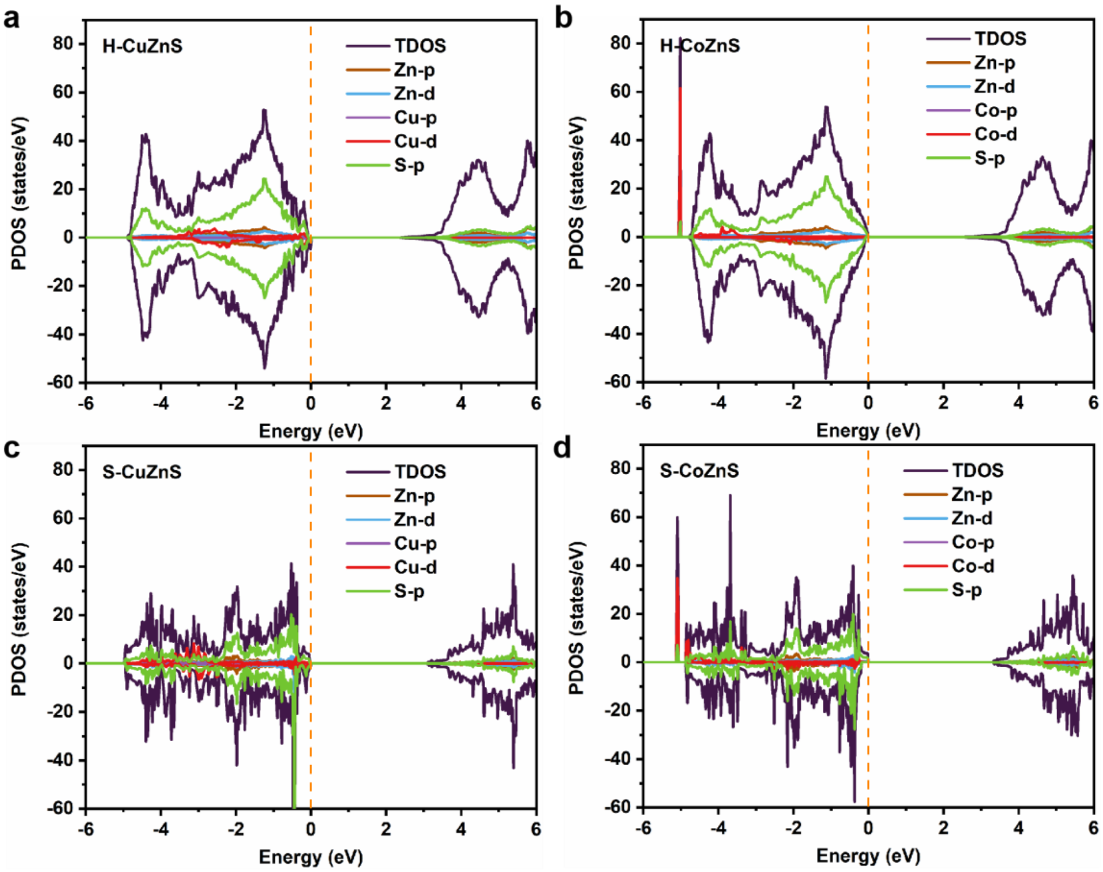

Figure S23. Density of states for (a) H-CuZnS, (b) H-CoZnS, (c) S-CuZnS, and (d) S-CoZnS.

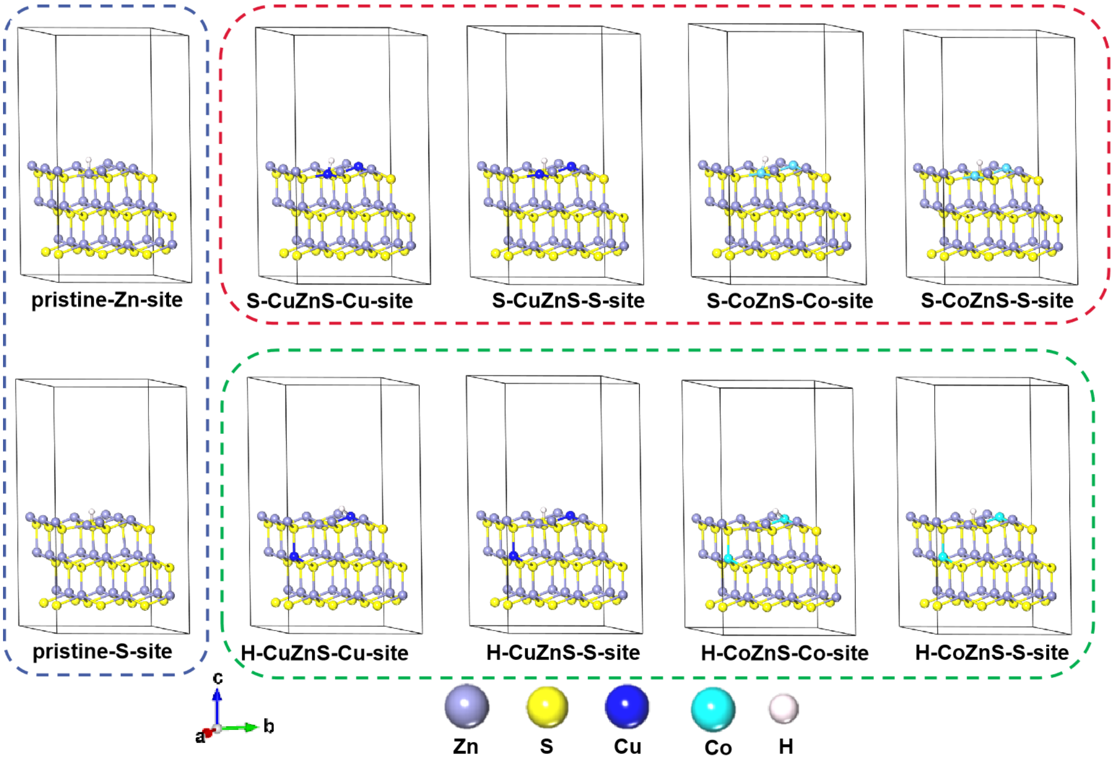

Figure S24. The corresponding optimized structures of H adsorption shown in Figure 3d in main text.

Table S4. DFT total energies (E_{DFT}), zero-point energies (E_{ZPE}), entropies multiplied by T (= 298.15 K) (TS), heat capacity ($\int C_p dT$) free energies (G), of HER intermediates at various sites of ZnS. All values are calculated in eV.

Species	E_{DFT}	E_{ZPE}	$\int C_p dT$	**TS**	**G**	**ΔG(H*)**
pristine-ZnS	-182.026	0.00	0.00	0.00	-182.026	
Zn-site (H*)	-186.341	0.164	0.017	0.025	-186.185	-0.709
S-site (H*)	-186.541	0.165	0.017	0.025	-186.384	-0.908
H-CuZnS	-175.239	0.00	0.00	0.00	-175.239	
Cu-site (H*)	-178.454	0.167	0.001	0.001	-178.287	0.402
S-site (H*)	-179.446	0.227	0.010	0.014	-179.223	-0.534
Zn-site (H*)	-177.380	0.165	0.009	0.014	-177.220	-1.981
S-CuZnS	-175.559	0.00	0.00	0.00	-175.559	
Cu-site (H*)	-178.991	0.152	0.009	0.014	-178.844	0.166
S-site (H*)	-179.625	0.182	0.010	0.012	-179.445	-0.435
H-CoZnS	-180.935	0.00	0.00	0.00	-180.935	
Co-site (H*)	-184.097	0.167	0.010	0.007	-183.927	0.458
S-site (H*)	-183.967	0.240	0.010	0.015	-183.732	0.653
S-CoZnS	-180.519	0.00	0.00	0.00	-180.519	
Co-site (H*)	-183.892	0.144	0.022	0.035	-183.761	0.209
S-site (H*)	-183.613	0.162	0.010	0.014	-183.455	0.515

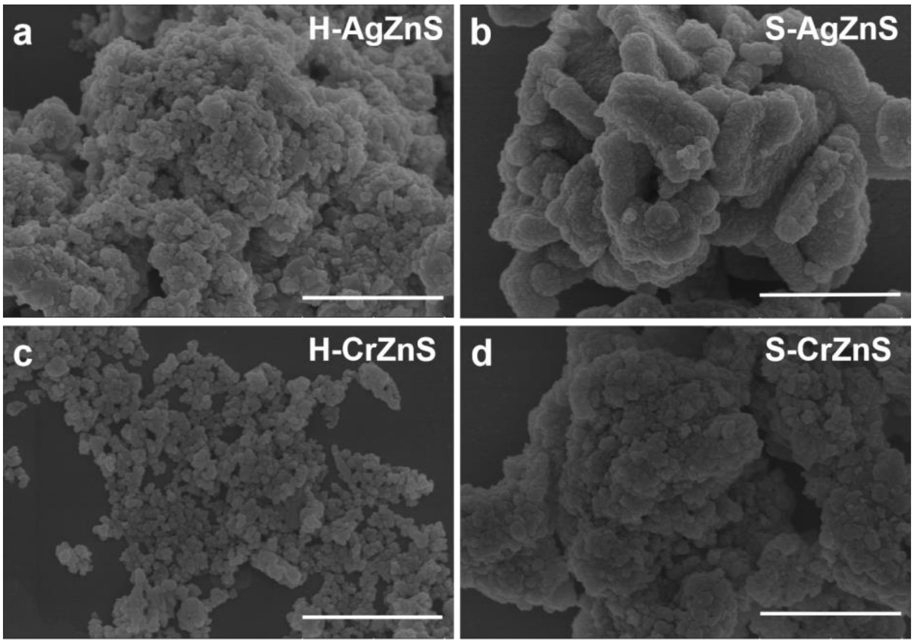

Figure S25. SEM images of (a) H-AgZnS, (b) S-AgZnS, (c) H-CrZnS, and (d) S-CrZnS, and the scale bar of the inset is 1 μm.

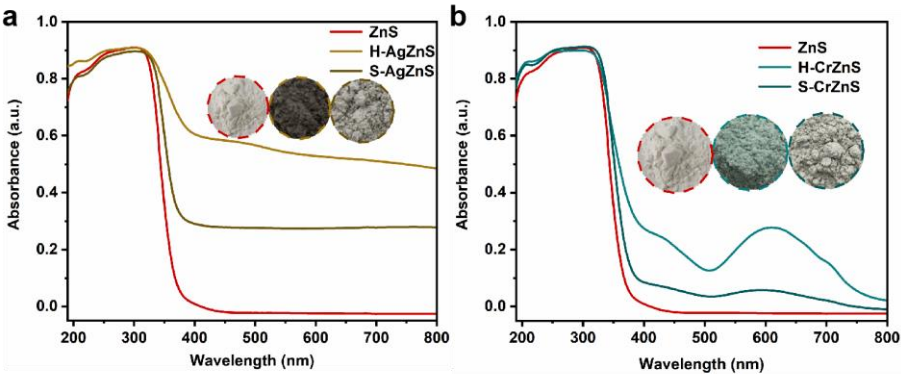

Figure S26. DRS spectra (the insets are the photograph of catalysts) for (a) ZnS, H-AgZnS, and S-AgZnS, (b) ZnS, H-CrZnS, and S-CrZnS.

Notes and references

1 G. Kresse, J. Furthmüller, *Comp. Mater. Sci.,* 1996, **6**, 15-50.

2 G. Kresse, J. Furthmüller, *Phys. Rev. B,* 1996, **54**, 11169-11186.

3 J. P. Perdew, A. Ruzsinszky, G. I. Csonka, O. A. Vydrov, G. E. Scuseria, L. A. Constantin, X. Zhou, K. Burke, *Phys. Rev. Lett.,* 2008, **100**, 136406.

4 S. Grimme, J. Antony, S. Ehrlich, H. Krieg, *J. Chem. Phys.,* 2010, **132**, 154104.

5 J. K. Nørskov, J. Rossmeisl, A. Logadottir, L. Lindqvist, J. R. Kitchin, T. Bligaard, H. Jónsson, *J. Phys. Chem. B,* 2004, **108**, 17886-17892.

6 S. K. Mandal, D. Karmakar, S. Ghosal, S. Paul, D. Jana, *ChemistrySelect,* 2019, **4**, 9102-9111.

7 Y. F. Liu, Y. H. Lv, Y. Y. Zhu, D. Liu, R. L. Zong, Y. F. Zhu, *Appl. Catal. B,* 2014, **147**, 851-857.

8 F. Su, H. Y. Peng, H. Yin, C. Luo, L. X. Zhu, W. Z. Zhong, L. Q. Mao, D. L. Yin, *J. Catal.,* 2021, **404**, 149-162.

9 J. Lee, S. Ham, D. Choi, D. J. Jang, *Nanoscale,* 2012, **00**, 1-3.

10 N. Zhang, Y. G. Luo, Y. H. Chen, J. Y. Zhang, H. Z. Wang, Z. J. Liu, *ACS Sustainable Chem. Eng.,* 2023, **11**, 4813-4824.

11 Y. Y. Li, J. S. Fan, R. Q. Tan, H. C. Yao, Y. Peng, Q. C. Liu, Z. J. Li, *ACS Appl. Mater. Interfaces,* 2020, **12**, 54507-54516.

12 C. Zeng, Y. M. Hu, T. R. Zhang, F. Dong, Y. H. Zhang, H. W. Huang, *J. Mater. Chem. A,* 2018, **6**, 16932-16942.